

Ultrafast simultaneous manipulation of multiple ferroic orders through nonlinear phonon excitation

Daniel A. Bustamante Lopez^{1†}, Dominik M. Juraschek^{2*†}, Michael Fechner³, Xianghan Xu⁴, Sang-Wook Cheong⁴ and Wanzheng Hu^{1,5*}

¹Department of Physics, Boston University, 590 Commonwealth Avenue, Boston, 02215, Massachusetts, USA.

²School of Physics and Astronomy, Tel Aviv University, 6997801, Tel Aviv, Israel.

³Max Planck Institute for the Structure and Dynamics of Matter, Center for Free-Electron Laser Science (CFEL), Luruper Chaussee 149, Hamburg, 22761, Germany.

⁴Rutgers Center for Emergent Materials and Department of Physics and Astronomy, Rutgers University, 136 Frelinghuysen Road, Piscataway, 08854, New Jersey, USA.

⁵Division of Materials Science and Engineering, Boston University, 590 Commonwealth Avenue, Boston, 02215, Massachusetts, USA.

*Corresponding author(s). E-mail(s): djuraschek@tauex.tau.ac.il; wanzheng@bu.edu;

Contributing authors: dabl@bu.edu;
michael.fechner@mpsd.mpg.de; xx8060@princeton.edu;
sangc@physics.rutgers.edu;

†These authors contributed equally to this work.

Abstract

Recent experimental studies have demonstrated the possibility of utilizing strong terahertz pulses to manipulate individual ferroic orders on pico- and femtosecond timescales. Here, we extend these findings and showcase the simultaneous manipulation of multiple ferroic orders in BiFeO₃, a material that is both ferroelectric and antiferromagnetic at room temperature. We find a concurrent enhancement of ferroelectric and antiferromagnetic second-harmonic generation (SHG) following the resonant excitation of a high-frequency fully-symmetric phonon mode. Based on first-principles calculations and phenomenological modeling, we ascribe this observation to the inherent coupling of the two ferroic

orders to the nonequilibrium distortions induced in the crystal lattice by nonlinearly driven phonons. Our finding highlights the potential of nonlinear phononics as a technique for manipulating multiple ferroic order parameters at once. In addition, this approach provides a promising avenue to studying the dynamical magnetization and polarization behavior, as well as their intrinsic coupling, on ultrashort timescales.

Keywords: multiferroics, nonlinear phononics, ultrafast dynamics

1 Introduction

Identifying efficient pathways to control the quantum phases of matter is a key challenge for the development of new materials with functional properties. In magnetoelectric multiferroics, the coupled magnetic and ferroelectric orders enable the control of magnetization using electric fields and vice versa, promising energy-efficient switching operations for data processing, and significant research efforts have been made to develop this concept within the last decade [1, 2]. BiFeO₃, shown in Fig. 1a, is a well-known multiferroic material at room temperature, whose ferroelectric polarization can be switched by an applied electric field, which is accompanied by a reorientation of its antiferromagnetic domain [3, 4]. While this magnetoelectric coupling is appealing for low-energy consumption spintronics [5, 6], the timescale of the switching process is limited by the ramp-up time of the applied electromagnetic fields, generally to nanosecond timescales.

In contrast, ultrashort laser pulses provide the possibility to generate large electric field strengths on sub-picosecond timescales, and recent experimental realizations of intense terahertz (THz) and mid-infrared (MIR) pulses with peak electric fields exceeding several megavolts per centimetre (MV/cm) have opened up new pathways for dynamical materials engineering [7, 8]. When the electric field component of a laser pulse is coupled resonantly to the dipole moment of an optical phonon mode, coherent lattice vibrations can be driven with amplitudes exceeding the harmonic regime, making anharmonic contributions of the interatomic potential-energy surface integral parts of the dynamics. A particular manifestation of this anharmonicity is nonlinear phononic rectification, a lattice analog to optical rectification, in which nonlinear coupling between phonon modes leads to a quasistatic distortion of the crystal structure [9–12], creating transient crystal geometries that are not accessible in equilibrium. Examples of nonlinear phononic rectification have achieved to manipulate and induce ferroelectric [13–17] and magnetic order [18–24] individually. It has so far remained unexplored however, whether light can control multiple ferroic order parameters simultaneously in a single domain.

Here, we coherently excite a high-frequency fully-symmetric (A_1) phonon mode in BiFeO₃ with intense MIR pulses and we probe the evolution of ferroelectricity and antiferromagnetism using time-resolved second-harmonic

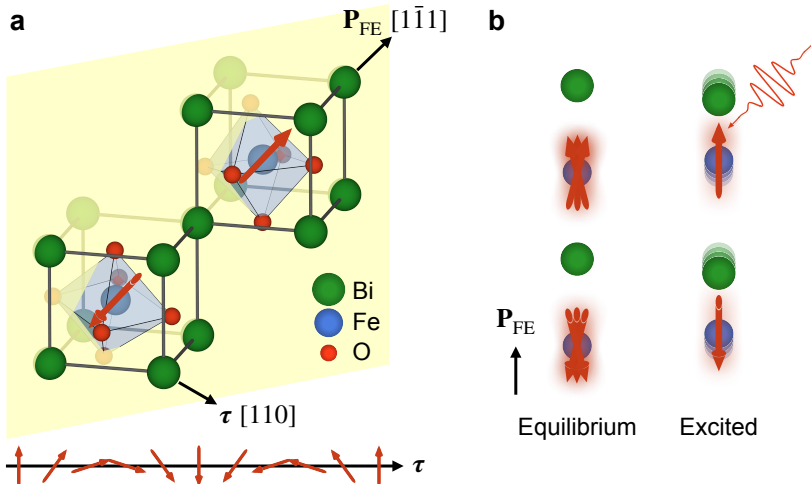


Fig. 1 Control of multiferroic order through nonlinear phonon dynamics.

a, Rhombohedral crystal structure of BiFeO₃ (space group $R3c$), in which the ferroelectric polarization (\mathbf{P}_{FE}) is along the stretched body-diagonal of the pseudocubic unit cell, identified as $[1\bar{1}\bar{1}]$ here. The spins between nearest-neighbor iron ions are antiferromagnetically aligned (red arrows) and form a spin cycloid with a wavelength of 62 nm along the normal vector τ of the mirror plane (yellow) [25, 26]. In a single-magnetic domain crystal, the spin cycloid breaks the three-fold rotation symmetry around \mathbf{P}_{FE} . **b**, (Left) Initial state with the equilibrium ferroelectric polarization and a thermal broadening of the iron-spin alignment. (Right) The lattice distortion following the resonant excitation of a A_1 phonon leads to a change in polarization and to an improved alignment of the iron spins.

generation (SHG) at room temperature. We find that both the ferroelectric and antiferromagnetic contributions to the SHG signal are enhanced on a sub-picosecond timescale. We perform phonon dynamics simulations supported by density functional theory calculations that predict a rectification of the A_1 modes arising from both three-phonon coupling and cubic anharmonicities, whose polar atomic displacements increase the magnitude of the ferroelectric contribution to the second-order nonlinear susceptibility tensor. Comparison with experimental data confirms that the total change in SHG signal contains a significant proportion of antiferromagnetic contribution, which we interpret as a stabilization of the antiferromagnetic state (Fig. 1b).

2 Results

2.1 Phonon-driven enhancement of second-harmonic generation

We study a single-crystal sample of BiFeO₃, cut and polished along the pseudocubic (110) plane. The ferroelectric polarization \mathbf{P}_{FE} is oriented along the body diagonal, $[1\bar{1}\bar{1}]$, which is parallel to the polished surface, as illustrated in Fig. 1a. Previous works show that the lattice, electronic, and magnetic degrees of freedom in BiFeO₃ are highly sensitive to external fields [25, 27–31]. The

large optical nonlinearities in BiFeO₃ [32] enables optical rectification that leads to coherent THz emission, which is a sensitive probe of the ferroelectric polarization [33]. We observed a pronounced angular dependence of the emitted THz field amplitude that verifies that our sample is predominantly in a single domain (Supplementary Information Section 1).

To control structural parameters critical to the ferroic properties, we used intense MIR pulses to excite the high-frequency A_1 mode in BiFeO₃ at 15.7 THz [34]. We used frequency-tunable MIR pulses with an excitation fluence of 12 mJ/cm² to couple to the electric dipole moment of the A_1 mode that is oriented along the ferroelectric polarization direction. Time-resolved SHG was used to probe the MIR-induced changes in the ferroic order parameters. The SHG intensity is proportional to the square of the light-induced nonlinear polarization, $I(2\omega) \propto |P(2\omega)|^2$. The transient state is characterized by the light-induced change in SHG intensity, $\Delta I(2\omega)$, with the probe polarization oriented parallel to the light scattering plane (angle $\phi = 0^\circ$) and the p -polarization detection configuration. A schematic of the pump-probe geometry is shown in Fig. 2a, indicating the atomic displacements induced by the high-frequency A_1 mode that are primarily composed of oxygen-ion motion. In Fig. 2b, we show the characterization of the MIR pump pulse and the polarization dependence of $\Delta I(2\omega)$. When the polarization of the MIR pulse is oriented along \mathbf{P}_{FE} , the SHG intensity is enhanced by 1.5%, whereas a polarization of the MIR pulse perpendicular to \mathbf{P}_{FE} yields no pump-induced change. When tuning the center frequency of the MIR pump pulse away from the A_1 phonon frequency, the pump-induced $\Delta I(2\omega)$ decays rapidly, as shown in Fig. 2c, indicating a resonant phonon-driven effect. Furthermore, the maximum transient change in polarization scales linearly with the pump fluence, shown in Fig. 2d, indicating a mechanism based on nonlinear phononic rectification and ionic Raman scattering [35].

SHG is a sensitive probe for ferroelectricity and magnetic ordering, as the symmetry of the material is reflected by the coefficients of the SHG susceptibility tensor that is given by

$$\mathbf{P}(2\omega) \propto \left(\chi^{(i)} + \chi^{(c)} \right) : \mathbf{E}(\omega) \otimes \mathbf{E}(\omega), \quad (1)$$

where $\mathbf{E}(\omega)$ is the electric field component of the laser pulse and $\chi^{(i)}$ and $\chi^{(c)}$ respectively are the ferroelectric and magnetic contributions to the SHG susceptibility tensor [36, 37]. The nonzero elements of the SHG tensors are determined by the point-group symmetry of the crystal. At room temperature, the crystal lattice of BiFeO₃ is rhombohedral with a $3m$ point-group symmetry (space group $R3c$). In the bulk, the antiferromagnetically aligned spins exhibit an additional long-range cycloidal modulation (Fig. 1a) that can be oriented along three equivalent wave vectors, commonly denoted by $(\boldsymbol{\tau}_1, \boldsymbol{\tau}_2, \boldsymbol{\tau}_3)$. The wave vectors $\boldsymbol{\tau}_i$ are perpendicular to \mathbf{P}_{FE} [25, 26]. Our sample is predominantly in a single ferroelectric domain, as well as a single spin-cycloid domain [25]. The uniqueness of the spin-cycloid wave vector lifts the three-fold rotation symmetry around \mathbf{P}_{FE} , and effectively lowers the symmetry of the system

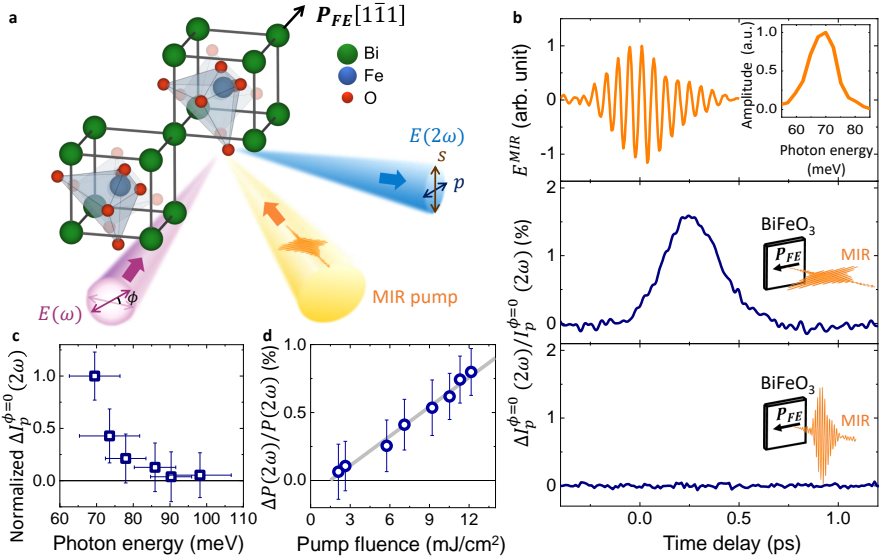


Fig. 2 Phonon-driven enhancement of second-harmonic generation. **a**, We used MIR pulses with a center frequency of 16.9 THz (69 meV) to drive the high-frequency A_1 phonon in BiFeO₃ at normal incidence. A probe beam at 800 nm was used for SHG with a 45° incidence in reflection geometry. **b**, (Top panel) Electric field component of the MIR pump and Fourier spectrum (inset). (Middle panel) The MIR pump induces a 1.5% transient enhancement of the SHG intensity when polarized along \mathbf{P}_{FE} . (Bottom panel) Rotating the MIR pump polarization by 90° results in no pump-probe signal. **c**, Dependence of the SHG signal on the center frequency of the MIR pump pulse. The signal becomes nonzero as the frequency of the pump pulse approaches that of the high-frequency A_1 mode, indicating a phonon-driven mechanism. **d**, Linear dependence of the light-induced change in second-harmonic polarization on the pump fluence, consistent with nonlinear phononic rectification and ionic Raman scattering [35].

to monoclinic, described by point group m . Because the ferroelectric and magnetic properties determine the point-group symmetry, information about them is intrinsically encoded in the symmetry and magnitude of the SHG tensor components that can be probed by varying the polarization of the probe beam.

In Figs. 3a and b, we show the probe-polarization dependence of the SHG signal in equilibrium. For the p -polarization detection, the SHG polar plot has two lobes at 0° and 180°, respectively. This can be fitted using nearly exclusively the $\chi^{(i)}$ tensor components (ferroelectric contribution, grey area). For the s -polarization detection, the SHG signal has four lobes, with a clear asymmetry along the 60° and 240° directions. This asymmetry is due to the nonzero $\chi^{(c)}$ tensor components (antiferromagnetic contribution, red area) arising from the symmetry lowering in the single spin-cycloid domain. Similar features were observed in BiFeO₃ thin films, in which the orientation of the asymmetric SHG component was used to identify different antiferromagnetic domains [38]. In Figs. 3c and d, we show the SHG polar plots in the phonon-driven state at the maximum of the pump-probe response. For both the p - and s -polarization detections, ΔI^{max} is anisotropic and primarily positive with

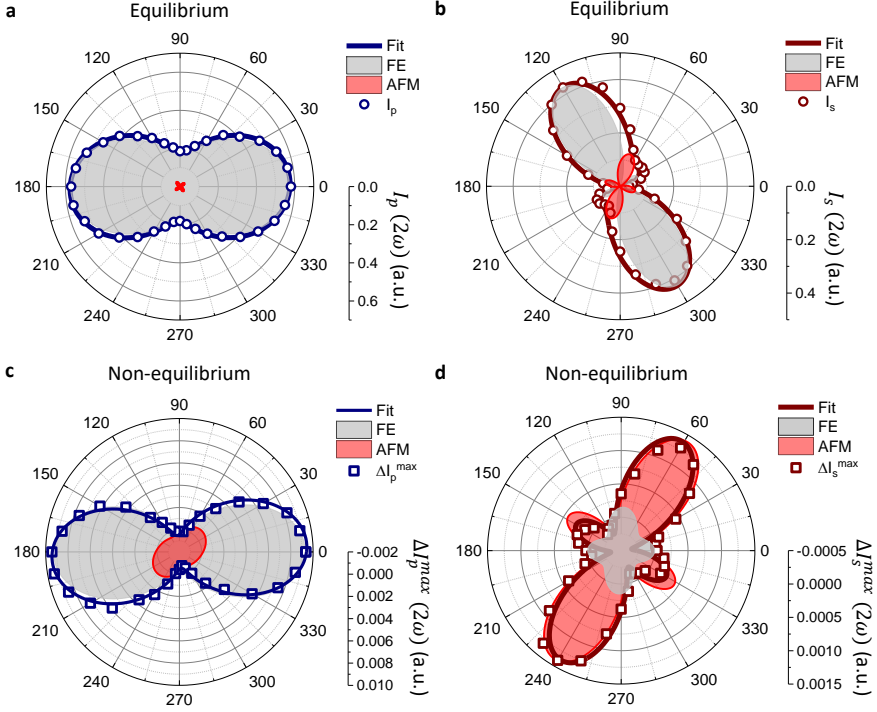


Fig. 3 Static and time-resolved SHG polarimetry. Polar plots of the equilibrium SHG intensity, I , are shown for **a**, p -polarization detection and **b**, s -polarization detection (open circles). Polar plots of the pump-induced change of the SHG intensity, ΔI , are shown for **c**, p -polarization detection and **d**, s -polarization detection at the maximum of the pump-probe response (open squares). In all plots, solid lines are fits of the SHG intensities, composed of the ferroelectric contribution (grey areas) and the antiferromagnetic contribution (red areas). Both the ferroelectric and antiferromagnetic contributions show an enhancement following the resonant phonon excitation.

varying probe polarization. The maximum enhancement for both $\Delta I_p^{max}/I_p$ and $\Delta I_s^{max}/I_s$ is approximately 1.5%. Intriguingly, the dominant contributions to the pump-induced p - and s -signal changes are from different χ tensors. In the p -detection channel, the maximum enhancement in SHG intensity is along 0° and 180° , given by the ferroelectric SHG tensor (grey area in Fig. 3c). In contrast, in the s -detection channel, the maximum enhancement in SHG intensity is along 60° and 240° , dominated by the antiferromagnetic SHG tensor (red area in Fig. 3d). In order to shed light on the physical mechanisms that lead to this simultaneous enhancement of ferroelectric and antiferromagnetic SHG enhancement, we perform simulations of the nonlinear phonon dynamics that follow the coherent excitation of the high-frequency A_1 mode by the MIR pulse.

2.2 Simulations of nonlinear phonon dynamics

We evaluate the nonlinear vibrational response and the corresponding lattice-polarization dynamics in a semi-classical oscillator model, for which we compute the input parameters from first principles using density functional theory. The point-group symmetry of BiFeO₃ allows for quadratic-linear three-phonon couplings of the resonantly driven high-frequency A_1 mode (calculated eigenfrequency 15.3 THz) to the three low-frequency A_1 modes (calculated eigenfrequencies 8.8, 7.4, and 4.8 THz) present in the system, which we denote as A_1^h and A_1^l in the following. The coupling is described by an interaction potential of $V = cQ_{A_1^h}^2 Q_{A_1^l}$, where Q is the phonon amplitude and c the coupling coefficient, and can be utilized for nonlinear phononic rectification: when the A_1^h mode is coherently driven, it enacts a unidirectional force on the A_1^l modes. This force induces a quasistatic displacement of the atoms along the eigenvectors of the A_1^l modes that is proportional to the mean-squared amplitude of the A_1^h mode, $\langle Q_{A_1^l} \rangle \propto \langle Q_{A_1^h}^2 \rangle$. Furthermore, as the high-frequency A_1 mode is driven with a large amplitude, it can experience self-rectification through cubic-order anharmonicity, described by the potential term $V = \tilde{c}Q_{A_1^h}^3$. Because all A_1 modes are infrared active, the rectification induces a quasistatic electric dipole moment and therefore an electric polarization in addition to the ferroelectric polarization. Details of the evolution of the phonon amplitudes according to the oscillator model and the density functional theory calculations of the coupling coefficients are provided in the Methods section and in the Supplementary Information Section 4.

In Fig. 4a, we show the displacements of the ions for the sum of the rectified components of all four A_1 modes. The cations, bismuth and iron, move in opposite directions along the [111] direction. In Fig. 4b, we show the transient polarization induced by the rectified components of all four A_1 modes, as well as the relative change of lattice polarization compared to the equilibrium ferroelectric polarization of 90 $\mu\text{C}/\text{cm}^2$. The rectifications of the individual A_1 modes induce opposing polarizations due to the opposite signs of their mode effective charges that lead to only a small net change in polarization, which can be explained by the opposite net motion of cations shown in Fig. 4a.

In order to predict the pump-induced change in SHG intensity, we calculate and compare the ferroelectric contribution to the SHG tensor components of both the equilibrium and transiently distorted lattice structures at the maximum of the vibrational response (see Supplementary Information Section 4 for computational details). In Figure 4c and d, we show the polar plots of the change in SHG intensity, ΔI , for the p - and s -detection channels that we obtain from the modified SHG tensor components due to nonlinear phononic rectification. The calculations well reproduce the experimental features (grey areas in Fig. 3c and d), which confirms the ferroelectric contribution to the SHG enhancement of ΔI_p , and supports the experimental finding that the enhancement of ΔI_s along 60° and 240° must stem from the antiferromagnetic $\chi^{(c)}$ tensor (red area in Fig. 3d).

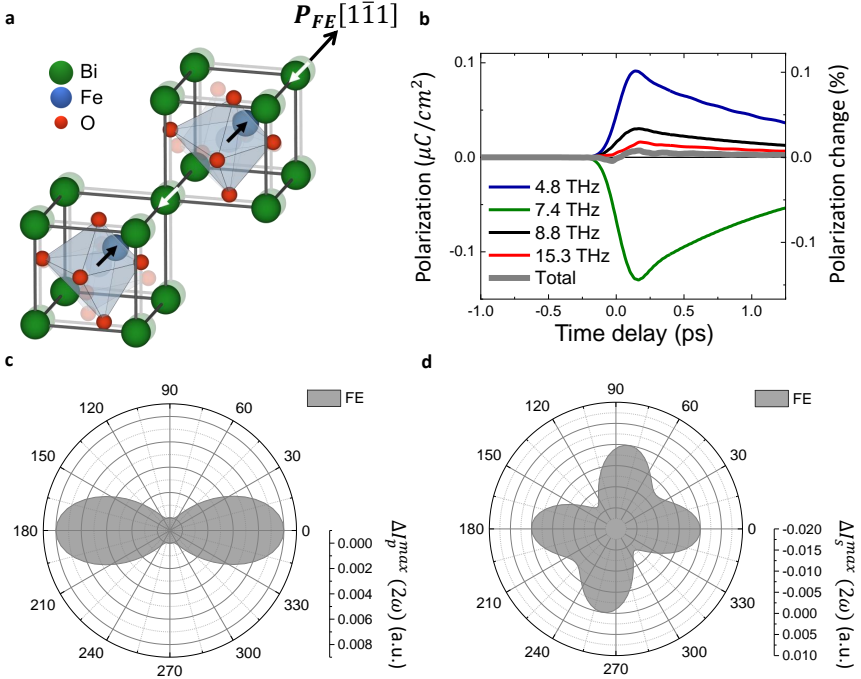


Fig. 4 Simulations of nonlinear phonon dynamics and phonon-induced ferroelectric SHG. **a**, Transient displacements of the ions along the rectified components of all four A_1 modes. Displacements are exaggerated for clarity. Besides the change in the oxygen octahedron, the two cations, bismuth and iron, move in opposite directions along the $[1\bar{1}1]$ direction, marked by black and white arrows. **b**, Polarization induced by the rectified components of the four A_1 modes, and percentile change of the electric polarization with respect to the equilibrium value ($90 \mu\text{C}/\text{cm}^2$). Calculated pump-induced changes in the SHG signal for the ferroelectric contribution are shown for **c**, p -polarization detection and **d**, s -polarization detection at the maximum response of the phonon amplitudes. The shape and magnitude of the polar plot in p -polarization fits excellently to the experimental data. In s -polarization, the shape of the experimental data for the ferroelectric contribution could be reproduced, however with an overestimation of the magnitude.

3 Discussion

We have demonstrated a simultaneous enhancement of ferroelectric and antiferromagnetic second-harmonic generation in BiFeO_3 by resonant excitation of a high-frequency fully-symmetric phonon mode. We stress that the pump-induced SHG intensity changes are not a multi-domain effect, as the single-crystal sample studied here is predominantly in a single ferroelectric and spin-cycloid domain [25]. The SHG signals from minor domains are negligible and do not match the experimental data, see Supplementary Information Section 3. We can further exclude the contribution from MIR-induced SHG, which involves the third-order susceptibility tensor, $\chi^{(3)}$. The $\chi^{(3)}$ signal is spectrally filtered (see Methods) and the $\chi^{(3)}$ process is spatially separated from the $\chi^{(2)}$ process due to the 45° angle between the SHG probe and the MIR

pump beams. In addition, the $\chi^{(3)}$ process would result in a quadratic pump fluence dependence for $\Delta P(2\omega)$, not the linear relation observed here (Fig. 2d).

The enhancement of the ferroelectric contribution can be well reproduced by our calculations of the $\chi^{(i)}$ tensor-component modulations due to the transient lattice distortion induced by nonlinear phononic rectification. Intriguingly, the lattice polarizations of the A_1 phonon have opposite signs due to the counter-phase motion of the cations along the direction of ferroelectric polarization, \mathbf{P}_{FE} , and nearly cancel each other out. In turn, they enhance the SHG tensor components directly, therefore leading to a larger $\mathbf{P}(2\omega)$ in comparison to the equilibrium state that our measurements pick up. While our theory captures the ferroelectric SHG features, the microscopic mechanism responsible for the enhancement of the antiferromagnetic contribution remains an open question, and we provide a number of possible explanations below that will have to be tested in the future.

A first possibility concerns phonon-induced changes of the exchange interaction, which have been described for a variety of magnetic systems in the past [18–20, 39]. The quasistatic distortion induced through nonlinear phononic rectification modifies the effective bond lengths and therefore potentially the exchange coupling that is inherently dependent on the distance between the atoms. As a result, this modification could lead to changes of the antiferromagnetic $\chi^{(c)}$ tensor components, similar to the ferroelectric case. The fully-symmetric A_1 modes that we drive by definition preserve the symmetry of the system and furthermore leave the relative distances between the iron ions mostly unchanged, however the relative distances between the iron and oxygen ions change, which affects the Dzyaloshinskii-Moriya interaction that is responsible for the noncollinear arrangement of spins in BiFeO_3 . A second possibility concerns phonon-induced symmetry breaking of the orbital configuration, which has recently been shown to stabilize magnetization above the ordering temperature in a transition-metal ferromagnet [40]. Due to the fully-symmetric nature of the A_1 modes, we can likely rule out this mechanism in our case. A third possibility concerns coherent magnon excitation through coupling to the phonons, which has in the past been described as ionic Raman scattering by magnons [41–43]. While ionic Raman scattering of the A_1 modes by the magnons might be possible in BiFeO_3 , only circularly polarized phonons would lead to a unidirectional force on the spins [44]. All A_1 modes involved in the dynamics are linearly polarized, and we therefore also rule out this mechanism for our case. Furthermore, the spectrum of our MIR pulse is far away from the electromagnon resonances in BiFeO_3 [45, 46], which allows us to exclude a coupling to the spins through the dipole moment of the spin cycloid. With the data and calculations given thus far, we therefore find it most likely that a modification of the exchange interactions leads to a stabilization of the antiferromagnetic order and to a change of the $\chi^{(c)}$ components.

4 Conclusion

To conclude, our results show that ultrashort pulses in the THz and MIR spectral range can be used to address multiple ferroic order parameters at once, utilizing the coupling to nonlinearly driven phonon modes. We have demonstrated simultaneous ferroelectric and antiferromagnetic SHG enhancement for the case of the prototypical multiferroic material BiFeO_3 , but we expect that this approach will be applicable generically to materials exhibiting magneto-electric coupling. The ferroic orders in BiFeO_3 form independently below the respective Curie and Néel temperatures at 1100 and 640 K. In so-called type-II multiferroics, in contrast, the ferroic orders are interdependent and emerge together, but these materials often suffer from very low multiferroic ordering temperatures [47]. An intriguing question therefore arises, whether both ferroic orders can be stabilized simultaneously above the multiferroic ordering temperature through coherent phonon excitation. This problem can be regarded in the same broad context as the light-induced stabilization of superconductivity, ferroelectricity, and magnetism demonstrated in recent experiments [15, 16, 40, 48, 49].

5 Methods

5.1 Crystal growth

The BiFeO_3 single crystal was grown using a traveling solvent technique in a Laser Floating Zone (LFZ) furnace [50]. Bi_2O_3 (99.975%, Alfa Aesar) and Fe_2O_3 (99.995%, Alfa Aesar) powder are mixed in molar ratio 1 : 1 and 4 : 1 for the feed rod and the traveling solvent, respectively. The feed rod material was sintered at 800°C for 20 hours with one intermediated grinding, and the solvent was sintered at 700°C for 5 hours. A 0.15 g solvent pellet was placed on top of the seed rod before starting the floating zone growth. The growth was performed in air, and the growth rate was 1 mm/h. The as-grown crystal is oriented by a Laue x-ray camera.

5.2 MIR pump-SHG probe setup

The fundamental beam for SHG is from a Ti:sapphire laser with a repetition rate of 1 kHz, energy of 30 nJ, and a duration of 40 fs. A schematic representation of the setup is shown in Fig. 5. A half-wave plate (HWP) was used to rotate the polarization of the fundamental beam. The beam was focused SHG signal was spectrally filtered by a band-pass filter, spatially filtered by an iris, and then detected by a photo-multiplier tube. A Glan-Taylor prism was used to select the desired polarization of the second-harmonic signal. All optical measurements were performed at room temperature, with a 45° incidence in reflection geometry.

MIR pump pulses with tunable wavelengths between 13 and 18.5 micron, and a duration of 250 fs were generated by optical parametric amplification and subsequent difference frequency generation in a GaSe crystal. The MIR

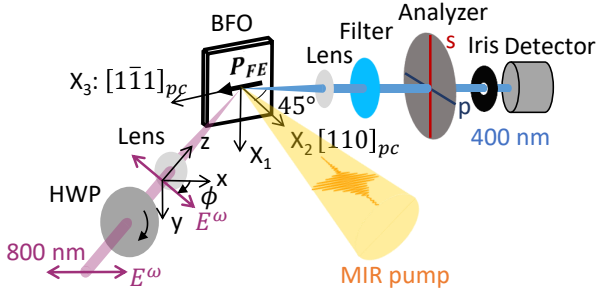


Fig. 5 Schematic of the MIR pump-SHG probe experiment, with the orientations of the (x, y, z) laboratory frame and the (X_1, X_2, X_3) crystal frame indicated. A half-wave plate (HWP) rotates the polarization of the 800 nm pulses. A dichroic mirror (not shown) reflects the second-harmonic generation signal and removes the residual 800 nm signal. A band-pass filter (10 nm bandwidth) removes signals from higher-order optical processes. An analyzer selects either the vertically polarized (s) or horizontally polarized (p) SHG signal.

pulses were focused on to the sample at normal incidence, with a diameter of 220 micron and a maximum excitation fluence of 12 mJ/cm^2 .

5.3 Fits of the SHG signal

At room temperature, BiFeO_3 crystallizes in rhombohedral symmetry with point group $3m$ and space group $R3c$. We set X_3 as the ferroelectric axis and X_2 as the normal to the mirror plane of the trigonal structure (Fig. 5). In a single antiferromagnetic domain, the long-range cycloidal modulation of the spin breaks the three-fold rotation symmetry around \mathbf{P}_{FE} , reducing the symmetry of the material to monoclinic with point group m . Details of the SHG tensors can be found in Supplementary Information Section 2. The fit reveals that the cycloidal spin modulation direction is along X_2 .

5.4 Theory of nonlinear phonon dynamics

We use a phenomenological oscillator model to evaluate the nonlinear vibrational response of the A_1 modes and the corresponding lattice-polarization dynamics following the excitation by an ultrashort MIR pulse, for which we compute all parameters from first principles using density functional theory. Specifically, we solve the equations of motion

$$\ddot{Q}_i + \kappa_i \dot{Q}_i + \partial_{Q_i} V = 0, \quad (2)$$

where Q_i are the normal mode coordinates (amplitudes) and κ_i the phenomenological linewidths of the A_1 modes in BiFeO_3 , $i \in \{A_1\}$. $V = V_0 + V_{\text{int}}$ is the potential energy, consisting of an equilibrium potential, V_0 , and an interaction potential, V_{int} . We expand V_0 up to fourth order in anharmonic and

nonlinear coupling terms,

$$V_0 = \sum_{i=\{A_1\}} \frac{\Omega_i^2}{2} Q_i^2 + \sum_{i,j,k=\{A_1\}} c_{ijk} Q_i Q_j Q_k + \sum_{i,j,k,l=\{A_1\}} d_{ijkl} Q_i Q_j Q_k Q_l, \quad (3)$$

where Ω_i is the phonon eigenfrequency, and c_{ijk} and d_{ijkl} are the anharmonic and nonlinear coupling coefficients. Because the A_1 modes are fully symmetric, all permutations of modes are allowed by symmetry in the anharmonic terms. We take into account all single-mode anharmonicities (c_{iii} , d_{iiii}), but only nonlinear couplings of the high-frequency A_1 (15.3 THz) mode, which is resonantly driven, to the other A_1 modes of the system. See Supplementary Information Section 4 for the density functional theory calculations of the coupling coefficients.

The interaction potential, V_{int} , contains the coupling of the electric dipole moment of the infrared-active phonon A_1 modes, p_i , to the electric field component of the laser pulse, $E(t)$, and can be written as

$$V_{\text{int}} = \sum_{i=\{A_1\}} p_i E(t) = \sum_{i=\{A_1\}} Z_i Q_i E(t), \quad (4)$$

where the linear polarization of the laser pulse is assumed to be aligned along the ferroelectric polarization direction of the crystal. Q_i is the phonon amplitude as evaluated in Eq. (2) and Z_i is the mode effective charge given by $Z_i = \sum_n Z_n^* q_{n,i} / \sqrt{M_n}$. Z_n^* is the Born effective charge tensor, $q_{n,i}$ the phonon eigenvector, and M_n the ionic mass of ion n , and the index n runs over all ions in the unit cell. We model the electric field component of the laser pulse as $E(t) = E_0 \exp[-t^2 / (2(\tau_0 / \sqrt{8 \ln 2})^2)] \cos(\omega_0 t)$ and set its parameters to the experimental values: a full width at half maximum (FWHM) duration of $\tau_0 = 250$ fs, a central frequency of $\omega_0 = 16.9$ THz, and a fluence of 12 mJ/cm² (peak electric field $E_0 = 5.3$ MV/cm). Because ω_0 is far off resonance from the three low-frequency A_1 modes, only the contribution of the A_1 (15.3 THz) mode plays a role in Eq. (4). Finally, the time-dependent electric polarization, $P(t)$, induced by the displacements of the ions along the coordinates of the infrared-active A_1 modes, is given by

$$P(t) = \sum_{i=\{A_1\}} p_i(t) / V_c, \quad (5)$$

where V_c is the volume of the unit cell.

We finally compute the phonon-induced modulation of the SHG tensor components. Due to the lack of inversion symmetry in the crystal, any infrared-active mode can linearly modify the components of $\chi^{(2)}$ as

$$\chi_{\text{pumped}}^{(2)}(t) = \chi_{\text{equilibrium}}^{(2)} + \sum_{j=\{A_1\}} \frac{\partial \chi_j^{(2)}}{\partial Q_j} Q_j(t). \quad (6)$$

Here, $\chi_{\text{equilibrium}}^{(2)}$ is the equilibrium second-order susceptibility and $\partial_{Q_j}\chi_j^{(2)}$ is the phonon-induced change. We compute both the equilibrium and nonequilibrium tensor components for the ferroelectric contribution, $\chi^{(i)}$, from first principles, see Supplementary Information Section 4.

Supplementary Information. Details of the SHG analysis and density functional theory calculations can be found in the Supplementary Information.

Acknowledgments. We acknowledge the helpful discussions with Liuyan Zhao, Ankit Disa, and Rui Zu. D.A.B.L. and W.H acknowledge support from the U.S. Department of Energy, Office of Science, Office of Basic Energy Sciences Early Career Research Program under Award Number DE-SC-0021305. The work at Rutgers was supported by the W.M. Keck Foundation. D.M.J. was supported by Tel Aviv University.

Author contributions. D.A.B.L. and D.M.J. contributed equally to this work. W.H. conceived the project, designed and performed the pump-probe measurements, and analyzed the data. D.A.B.L. performed data fitting and modeling. D.M.J. performed the density functional theory calculations and simulations of the nonlinear phonon dynamics. M.F. performed the density functional theory calculations of the SHG tensor components. X.X. and S-W.C. grew the sample. W.H. and D.M.J. wrote the paper with input from all other authors.

Declarations

All authors declare no competing interests.

References

- [1] Eerenstein, W., Mathur, N.D., Scott, J.F.: Multiferroic and magnetoelectric materials. *Nature* **442**, 759–765 (2006). <https://doi.org/10.1038/nature05023>
- [2] Spaldin, N.A., Ramesh, R.: Advances in magnetoelectric multiferroics. *Nat. Mater.* **18**, 203–212 (2019). <https://doi.org/10.1038/s41563-018-0275-2>
- [3] Zhao, T., Scholl, A., Zawaliche, F., Lee, K., Barry, M., Doran, A., Cruz, M.P., Chu, Y.H., Ederer, C., Spaldin, N.A., Das, R.R., Kim, D.M., Baek, S.H., Eom, C.B., Ramesh, R.: Electrical control of antiferromagnetic domains in multiferroic BiFeO₃ films at room temperature. *Nat. Mater.* **5**, 823–829 (2006). <https://doi.org/10.1038/nmat1731>
- [4] Lebeugle, D., Colson, D., Forget, A., Viret, M., Bataille, A.M., Gukasov, A.: Electric-field-induced spin flop in BiFeO₃ single crystals at room temperature. *Phys. Rev. Lett.* **100**, 227602 (2008). <https://doi.org/10.1103/PhysRevLett.100.227602>

- [5] Heron, J.T., Trassin, M., Ashraf, K., Gajek, M., He, Q., Yang, S.Y., Nikonov, D.E., Chu, Y.-H., Salahuddin, S., Ramesh, R.: Electric-field-induced magnetization reversal in a ferromagnet-multiferroic heterostructure. *Phys. Rev. Lett.* **107**, 217202 (2011). <https://doi.org/10.1103/PhysRevLett.107.217202>
- [6] Heron, J.T., Bosse, J.L., He, Q., Gao, Y., Trassin, M., Ye, L., Clarkson, J.D., Wang, C., Liu, J., Salahuddin, S., Ralph, D.C., Schlom, D.G., Íñiguez, J., Huey, B.D., Ramesh, R.: Deterministic switching of ferromagnetism at room temperature using an electric field. *Nature* **516**, 370–373 (2014). <https://doi.org/10.1038/nature14004>
- [7] Liu, B., Bromberger, H., Cartella, A., Gebert, T., Först, M., Cavalleri, A.: Generation of narrowband, high-intensity, carrier-envelope phase-stable pulses tunable between 4 and 18 THz. *Opt. Lett.* **42**, 129–131 (2017). <https://doi.org/10.1364/OL.42.000129>
- [8] Vicario, C., Trisorio, A., Allenspach, S., Rüegg, C., Giorgianni, F.: Narrow-band and tunable intense terahertz pulses for mode-selective coherent phonon excitation. *Appl. Phys. Lett.* **117**, 101101 (2020). <https://doi.org/10.1063/5.0015612>
- [9] Först, M., Manzoni, C., Kaiser, S., Tomioka, Y., Tokura, Y., R., M., Cavalleri, A.: Nonlinear phononics as an ultrafast route to lattice control. *Nat. Phys.* **7**, 854–856 (2011). <https://doi.org/10.1038/nphys2055>
- [10] Subedi, A., Cavalleri, A., Georges, A.: Theory of nonlinear phononics for coherent light control of solids. *Phys. Rev. B* **89**, 220301 (2014). <https://doi.org/10.1103/PhysRevB.89.220301>
- [11] Fechner, M., Spaldin, N.A.: Effects of intense optical phonon pumping on the structure and electronic properties of yttrium barium copper oxide. *Phys. Rev. B* **94**, 134307 (2016). <https://doi.org/10.1103/PhysRevB.94.134307>
- [12] Juraschek, D.M., Fechner, M., Spaldin, N.A.: Ultrafast Structure Switching through Nonlinear Phononics. *Phys. Rev. Lett.* **118**, 054101 (2017). <https://doi.org/10.1103/PhysRevLett.118.054101>
- [13] Subedi, A.: Proposal for ultrafast switching of ferroelectrics using midinfrared pulses. *Phys. Rev. B* **92**, 214303 (2015). <https://doi.org/10.1103/PhysRevB.92.214303>
- [14] Mankowsky, R., von Hoegen, A., Först, M., Cavalleri, A.: Ultrafast Reversal of the Ferroelectric Polarization. *Phys. Rev. Lett.* **118**, 197601 (2017). <https://doi.org/10.1103/PhysRevLett.118.197601>

- [15] Nova, T., Disa, A., Fechner, M., Cavalleri, A.: Metastable ferroelectricity in optically strained SrTiO₃. *Science* **364**, 1075–1079 (2019). <https://doi.org/10.1126/science.aaw4911>
- [16] Li, X., Qiu, T., Zhang, J., Baldini, E., Lu, J., Rappe, A.M., Nelson, K.A.: Terahertz field-induced ferroelectricity in quantum paraelectric SrTiO₃. *Science* **364**, 1079–1082 (2019). <https://doi.org/10.1126/science.aaw4913>
- [17] Chen, P., Paillard, C., Zhao, H.J., Íñiguez, J., Bellaiche, L.: Deterministic control of ferroelectric polarization by ultrafast laser pulses. *Nat. Commun.* **13**, 2566 (2022). <https://doi.org/10.1038/s41467-022-30324-5>
- [18] Fechner, M., Sukhov, A., Chotorlishvili, L., Kenel, C., Berakdar, J., Spaldin, N.A.: Magnetophononics: Ultrafast spin control through the lattice. *Phys. Rev. Materials* **2**, 064401 (2018). <https://doi.org/10.1103/PhysRevMaterials.2.064401>
- [19] Khalsa, G., Benedek, N.A.: Ultrafast optically induced ferromagnetic/anti-ferromagnetic phase transition in GdTio₃ from first principles. *npj Quantum Mater.* **3**, 15 (2018). <https://doi.org/10.1038/s41535-018-0086-3>
- [20] Rodriguez-Vega, M., Lin, Z.-X., Leonardo, A., Ernst, A., Chaudhary, G., Vergniory, M.G., Fiete, G.A.: Phonon-mediated dimensional crossover in bilayer CrI₃. *Phys. Rev. B* **102**, 081117 (2020). <https://doi.org/10.1103/physrevb.102.081117>
- [21] Disa, A.S., Fechner, M., Nova, T.F., Liu, B., Först, M., Prabhakaran, D., Radaelli, P.G., Cavalleri, A.: Polarizing an antiferromagnet by optical engineering of the crystal field. *Nat. Phys.* **16**, 937–941 (2020). <https://doi.org/10.1038/s41567-020-0936-3>
- [22] Afanasiev, D., Hortensius, J.R., Ivanov, B.A., Sasani, A., Bousquet, E., Blanter, Y.M., Mikhaylovskiy, R.V., Kimel, A.V., Caviglia, A..D.: Ultrafast control of magnetic interactions via light-driven phonons. *Nat. Mater.* **20**, 607 (2021). <https://doi.org/10.1038/s41563-021-00922-7>
- [23] Stupakiewicz, A., Davies, C.S., Szerenos, K., Afanasiev, D., Rabinovich, K.S., Boris, A.V., Caviglia, A., Kimel, A.V., Kirilyuk, A.: Ultrafast phononic switching of magnetization. *Nat. Phys.* **17**, 489 (2021). <https://doi.org/10.1038/s41567-020-01124-9>
- [24] Disa, A.S., Nova, T.F., Cavalleri, A.: Engineering crystal structures with light. *Nat. Phys.* **17**, 1087–1092 (2021). <https://doi.org/10.1038/s41567-021-01366-1>
- [25] Lee, S., Choi, T., Ratcliff II, W., Erwin, R., Cheong, S.-W., Kiryukhin,

- V.: Single ferroelectric and chiral magnetic domain of single-crystalline BiFeO₃ in an electric field. *Phys. Rev. B* **78**, 100101 (2008). <https://doi.org/10.1103/PhysRevB.78.100101>
- [26] Ratchiff, W., Lynn, J.W., Kiryukhin, V., Jain, P., Fitzsimmons, M.R.: Magnetic structures and dynamics of multiferroic systems obtained with neutron scattering. *npj Quantum Materials* **1**, 16003 (2016). <https://doi.org/10.1038/npjquantmats.2016.3>
- [27] Choi, T., Lee, S., Choi, Y.J., Kiryukhin, V., Cheong, S.-W.: Switchable ferroelectric diode and photovoltaic effect in BiFeO₃. *Science* **324**, 63 (2009). <https://doi.org/10.1126/science.1168663>
- [28] Kundys, B., Viret, M., Colson, D., Kundys, D.O.: Light-induced size changes in BiFeO₃ crystals. *Nat. Mater.* **9**, 803 (2010). <https://doi.org/10.1038/nmat2807>
- [29] Chen, F., Goodfellow, J., Liu, S., Grinberg, I., Hoffmann, M.C., Damodaran, A.R., Zhu, Y., Zalden, P., Zhang, X., Takeuchi, I., Rappe, A.M., Martin, L.W., Wen, H., Lindenberg, A.M.: Ultrafast terahertz gating of the polarization and giant nonlinear optical response in BiFeO₃ thin films. *Adv. Mater.* **27**, 6371 (2015). <https://doi.org/10.1002/adma.201502975>
- [30] Rubio-Marcos, F., Ochoa, D.A., Del Campo, A., García, M.A., Castro, G.R., Fernández, J.F., García, J.E.: Reversible optical control of macroscopic polarization in ferroelectrics. *Nature Photon.* **12**, 29–32 (2018). <https://doi.org/10.1038/s41566-017-0068-1>
- [31] Liou, Y.-D., Chiu, Y.-Y., Hart, R.T., Kuo, C.-Y., Huang, Y.-L., Wu, Y.-C., Chopdekar, H.-J. R. V. and Liu, Tanaka, A., Chen, C.-T., Chang, C.-F., Tjeng, L.H., Cao, Y., Nagarajan, V., Chu, Y.-H., Chen, Y.-C., Yang, J.-C.: Deterministic optical control of room temperature multiferroicity in BiFeO₃ thin films. *Nat. Mater.* **18**, 580–587 (2019). <https://doi.org/10.1038/s41563-019-0348-x>
- [32] Kumar, A., Rai, R.C., Podraza, N.J., Denev, S., Ramirez, M., Chu, Y.-H., Martin, L.W., Ihlefeld, J., Heeg, T., Schubert, J., Schlom, D.G., Orenstein, J., Ramesh, R., Collins, R.W., Musfeldt, J.L., Gopalan, V.: Linear and nonlinear optical properties of BiFeO₃. *Appl. Phys. Lett.* **92**, 121915 (2008). <https://doi.org/10.1063/1.2901168>
- [33] Talbayev, D., Lee, S., Cheong, S.-W., Taylor, A.J.: Terahertz wave generation via optical rectification from multiferroic BiFeO₃. *Appl. Phys. Lett.* **93**, 212906 (2008). <https://doi.org/10.1063/1.3036526>
- [34] Palai, R., Schmid, H., Scott, J.F., Katiyar, R.S.: Raman spectroscopy

- of single-domain multiferroic BiFeO₃. *Phys. Rev. B* **81**, 064110 (2010). <https://doi.org/10.1103/PhysRevB.81.064110>
- [35] Neugebauer, M.J., Juraschek, D.M., Savoini, M., Engeler, P., Boie, L., Abreu, E., Spaldin, N.A., Johnson, S.L.: Comparison of coherent phonon generation by electronic and ionic Raman scattering in LaAlO₃. *Phys. Rev. Research* **3**, 13126 (2021). <https://doi.org/10.1103/physrevresearch.3.013126>
- [36] Denev, S.A., Lummen, T.T.A., Barnes, E., Kumar, A., Gopalan, V.: Probing ferroelectrics using optical second harmonic generation. *J. Am. Ceram. Soc.* **94**, 2699–2727 (2011). <https://doi.org/10.1111/j.1551-2916.2011.04740.x>
- [37] Fiebig, M., Pavlov, V.V., Pisarev, R.V.: Second-harmonic generation as a tool for studying electronic and magnetic structures of crystals: review. *J. Opt. Soc. Am. B* **22**, 96–118 (2005). <https://doi.org/10.1364/JOSAB.22.000096>
- [38] Chauleau, J.-Y., Haltz, E., Carrétéro, C., Fusil, S., Viret, M.: Multi-stimuli manipulation of antiferromagnetic domains assessed by second-harmonic imaging. *Nat. Matter.* **16**, 803–807 (2017). <https://doi.org/10.1038/nmat4899>
- [39] Padmanabhan, H., Poore, M., Kim, P.K., Koocher, N.Z., Stoica, V.A., Puggioni, D., Wang, H., Shen, X., Reid, A.H., Gu, M., Wetherington, M., Lee, S.H., Schaller, R.D., Mao, Z., Lindenberg, A.M., Wang, X., Rondinelli, J.M., Averitt, R.D., Gopalan, V.: Interlayer magnetophononic coupling in MnBi₂Te₄. *Nat. Commun.* **13**, 1929 (2022). <https://doi.org/10.1038/s41467-022-29545-5>
- [40] Disa, A.S., Curtis, J., Fechner, M., Liu, A., Hoegen, A., Först, M., Nova, T.F., Narang, P., Maljuk, A., Boris, A.V., Keimer, B., Cavalleri, A.: Photo-induced high-temperature ferromagnetism in YTiO₃. *Nature* **617**, 73 (2023). <https://doi.org/10.1038/s41586-023-05853-8>
- [41] Nova, T.F., Cartella, A., Cantaluppi, A., Först, M., Bossini, D., Mikhaylovskiy, R.V., Kimel, A.V., Merlin, R., Cavalleri, A.: An effective magnetic field from optically driven phonons. *Nat. Phys.* **13**, 132–137 (2017). <https://doi.org/10.1038/nphys3925>
- [42] Juraschek, D.M., Fechner, M., Balatsky, A.V., Spaldin, N.A.: Dynamical multiferroicity. *Phys. Rev. Mater.* **1**, 014401 (2017). <https://doi.org/10.1103/PhysRevMaterials.1.014401>
- [43] Juraschek, D.M., Narang, P., Spaldin, N.A.: Phono-magnetic analogs to opto-magnetic effects. *Phys. Rev. Research* **2**, 043035 (2020). <https://doi.org/10.1103/PhysRevResearch.2.043035>

[org/10.1103/PhysRevResearch.2.043035](https://doi.org/10.1103/PhysRevResearch.2.043035)

- [44] Juraschek, D.M., Neuman, T., Narang, P.: Giant effective magnetic fields from optically driven chiral phonons in 4f paramagnets. *Phys. Rev. Research* **4**, 013129 (2022). <https://doi.org/10.1103/PhysRevResearch.4.013129>
- [45] De Sousa, R., Moore, J.E.: Optical coupling to spin waves in the cycloidal multiferroic BiFeO₃. *Phys. Rev. B* **77**, 012406 (2008). <https://doi.org/10.1103/PhysRevB.77.012406>
- [46] Cazayous, M., Gallais, Y., Sacuto, A., De Sousa, R., Lebeugle, D., Colson, D.: Possible observation of cycloidal electromagnons in BiFeO₃. *Phys. Rev. Lett.* **101**, 037601 (2008). <https://doi.org/10.1103/PhysRevLett.101.037601>
- [47] Cheong, S.-W., Mostovoy, M.: Multiferroics: a magnetic twist for ferroelectricity. *Nat. Mater.* **6**, 13–20 (2007). <https://doi.org/10.1038/nmat1804>
- [48] Mankowsky, R., Subedi, A., Först, M., Mariager, S.O., Chollet, M., Lemke, H.T., Robinson, J.S., Glowia, J.M., Minitti, M.P., Frano, A., Fechner, M., Spaldin, N.A., Loew, T., Keimer, B., Georges, A., Cavalleri, A.: Nonlinear lattice dynamics as a basis for enhanced superconductivity in YBa₂Cu₃O_{6.5}. *Nature* **516**, 71–73 (2014). <https://doi.org/10.1038/nature13875>
- [49] Mitrano, M., Cantaluppi, A., Nicoletti, D., Kaiser, S., Perucchi, A., Lupi, S., Di Pietro, P., Pontiroli, D., Riccò, M., Clark, S.R., Jaksch, D., Cavalleri, A.: Possible light-induced superconductivity in K₃C₆₀ at high temperature. *Nature* **530**, 461–464 (2016). <https://doi.org/10.1038/nature16522>
- [50] Ito, T., Ushiyama, T., Yanagisawa, Y., Kumai, R., Tomioka, Y.: Growth of highly insulating bulk single crystals of multiferroic BiFeO₃ and their inherent internal strains in the domain-switching process. *Cryst. Growth Des.* **11**, 5139–5143 (2011). <https://doi.org/10.1021/cg201068m>